Environmental Research Letters

Supplementary Information for

Non-uniform seasonal warming regulates vegetation greening and atmospheric CO_2 amplification over northern lands

Contents of this file

Text S1
Figures S1 to S11
Tables S1 to S5

Introduction

This *Supplemental Information* **presents figures and tables supporting the document:**

- Text S1. FLUXCOM TER
- Figure S1. Seasonal curves of atmospheric CO_2 concentration (black) and NDVI (blue) in the northern lands (>50 °N).
- Figure S2. Temporal variations of the atmospheric $[CO_2]_{amplitude}$ collected from 4 processing methods
- Figure S3. Changes in temporal trends of atmospheric CO_2 amplitude and NDVI with 15-year moving windows.
- Figure S4. Changes in temporal trends of atmospheric CO_2 amplitude and NDVI with 20-year moving windows.
- Figure S5. Temporal variation of seasonal $[CO_2]_{amplitude}$, $[CO_2]_{min}$, $[CO_2]_{max}$, NDVI, GPP (MTE), growing season NEE in northern lands (>50 °N) during 1982-2010.
- Figure S6. The correlation between NDVI and GSL in temporal and spatial scales.
- Figure S7. Response of SOS and EOS to seasonal temperature in northern high latitude during 1982-2010.
- Figure S8. The temporal dynamics of NDVI and phenological metrics in northern high latitudes during 1982-2010.
- Figure S9. The partial correlation coefficient (partial *r*) of NDVI and model GPP to spring temperature
- Figure S10. The partial correlation coefficient (partial *r*) of NDVI and model GPP to autumn temperature

- Figure S11. The trends of seasonal respiration over northern lands (>50 °N) during the whole studied periods (1982-2010) and the special periods (1993-2007).
- Table S1. Information of the ensemble terrestrial ecosystem models
- Table S2. The 10-year moving trend of $[CO_2]_{amplitude}$, $[CO_2]_{max}$ and $[CO_2]_{min}$ at BRW over 1982-2010.
- Table S3. The 15-year moving trend of $[CO_2]_{amplitude}$, $[CO_2]_{max}$ and $[CO_2]_{min}$ at BRW over 1982-2010.
- Table S4. The changing trends of seasonal temperature from 1982 to 2010 across 15-year intervals.
- Table S5. The changing trends of GSL, SOS and EOS during 1982-2010 by 15-year intervals.

21 **pages (including cover page)**

Text S1 FLUXCOM TER.

The FLUXCOM TER were up scaled from FLUXNET-based in situ carbon flux estimates (Reichstein et al., 2005, Lasslop et al., 2010) using three machine learning algorithms (Papale and Valentini 2003), artificial neural networks (ANNs, Papale and Valentini 2003), random forest (RF, Tramontana et al., 2015) and model trees ensemble (MTE, Jung et al., 2011). To upscale the data, gridded meteorological measurements (e.g. daily air temperature, water availability and radiation) and satellite data were used to train the three models. In processing the global gridded products, two partitioning methods (Reichstein et al., 2005, Lasslop et al., 2010) of carbon flux estimates were used. Combining with these three fitting algorithms, it provided six sets of GPP and TER estimates each (Jung et al., 2017), which could be accessed from the Data Portal of the Max Planck Institute for the Biogeochemistry (https://www.bgc-jena.mpg.de/geodb/projects/Home.php). The daily TER of all ensemble means were used to produce growing season and non-growing season TER to calculate the changed rates during 1993-2007 comparing the period of 1982-2010 in figure S9. The trends of seasonal respiration were first calculated at each grid with Theil-Sen estimator, then the gridded trend were averaged to regional levels. And the difference between 1982-2010 and 1993-2007 were estimated by One-way ANOVA.

Figure S1. Seasonal curves of atmospheric CO_2 concentration (black) and NDVI (blue) in the northern lands (>50 °N). The monthly values are calculated as the 29-year average across 1982 to 2010. The green shade area marks the growing season averaging from 1982-2010.

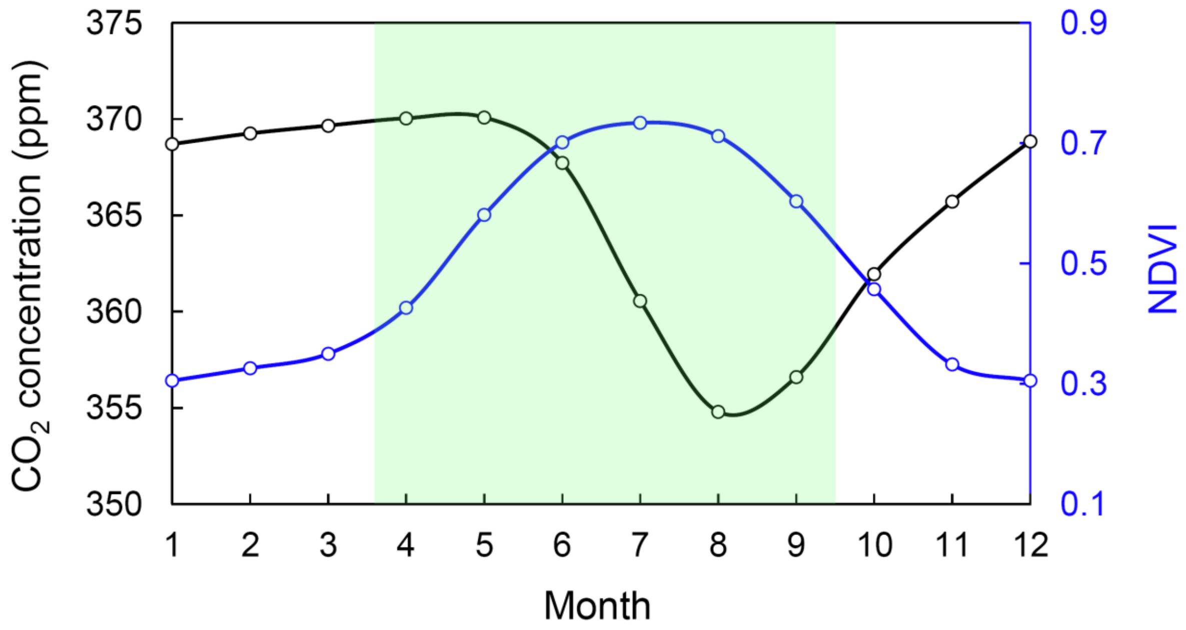

Figure S2. Temporal variations of the atmospheric $[CO_2]_{amplitude}$ calculating by four different processing methods (see section 2.1). In each panel, the disperse dots showed the anomalies of each metrics, the dashed black line with the grey shade areas indicated the 5-year dynamics (mean ±1 S.D.). The long-term trends of $[CO_2]_{amplitude}$ during 1982-2010 were estimated by Theil-Sen estimator which were shown by the red lines.

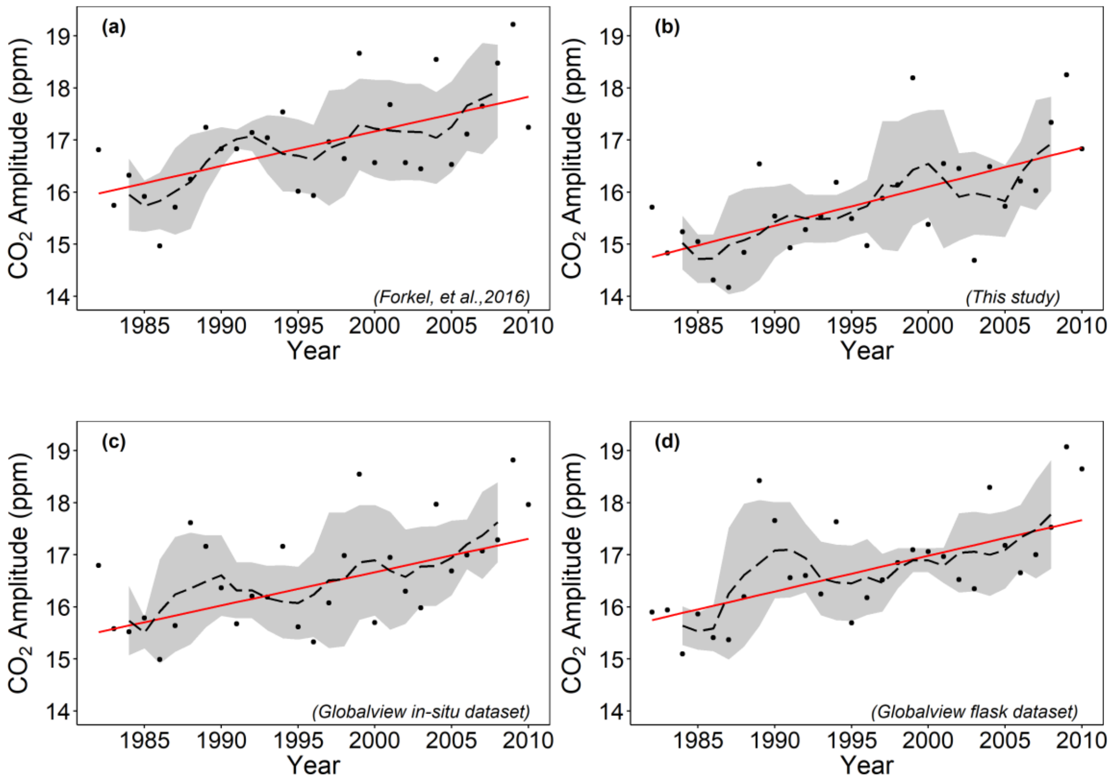

Figure S3. Changes in temporal trends of atmospheric CO_2 amplitude and plant greenness (NDVI). 15-year moving window from 1982 to 2010 show the changing trends of (a) annual amplitude ($[CO_2]_{amplitude}$), minimum ($[CO_2]_{min}$) and maximum ($[CO_2]_{max}$) of atmospheric CO_2 concentration ($[CO_2]$) recorded from Point Barrow (BRW); (b) NDVI and growing season length (GSL). Because decreased $[CO_2]_{min}$ contributes positive effect on enhanced $[CO_2]_{amplitude}$, we show the subtractive $[CO_2]_{min}$ trends in panel (a).

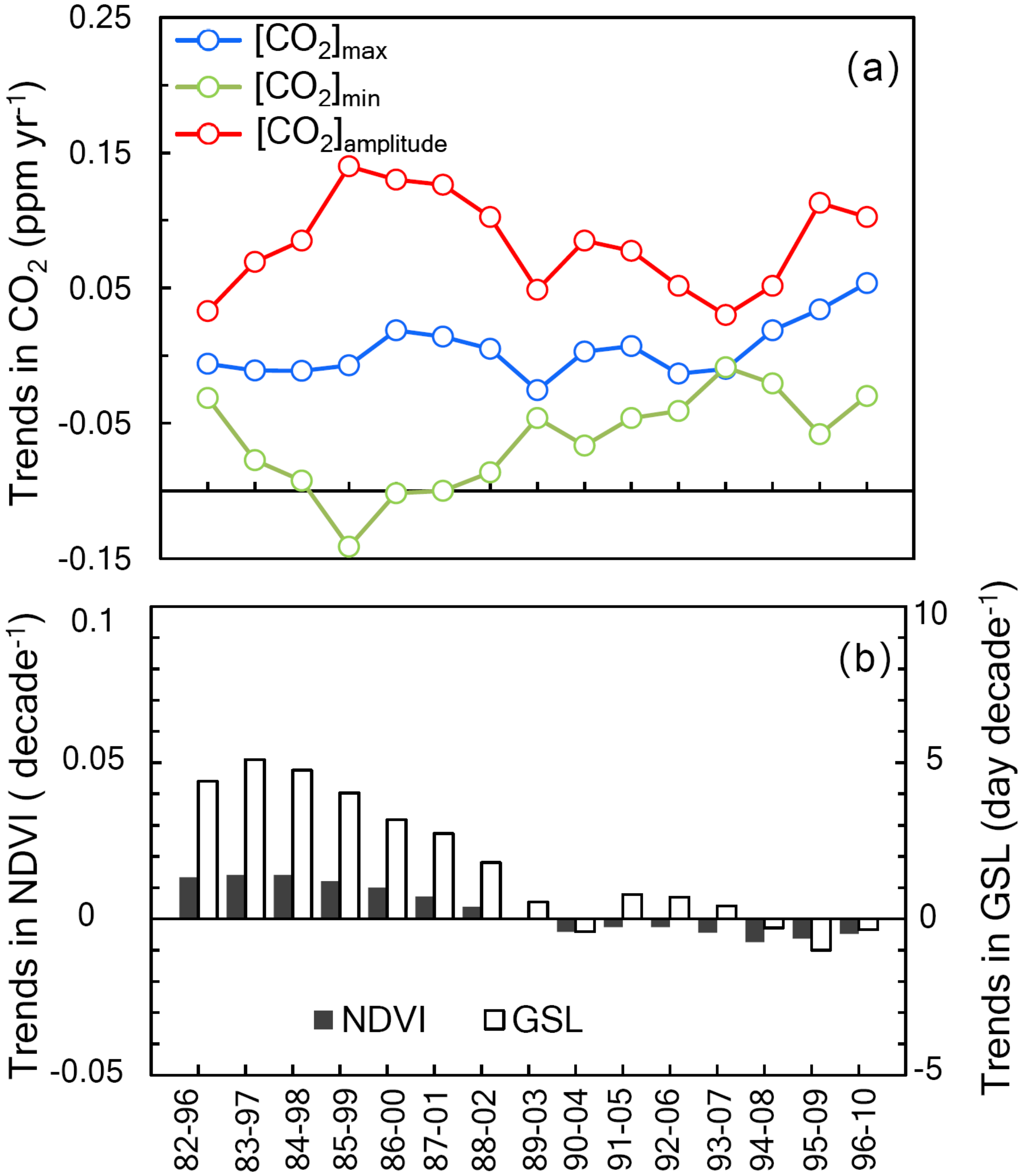

Figure S4. Changes in temporal trends of atmospheric CO_2 amplitude and plant greenness (NDVI). 20-year moving windows from 1982 to 2010 show the changing trends of (a) annual amplitude ($[CO_2]_{amplitude}$), minimum ($[CO_2]_{min}$) and maximum ($[CO_2]_{max}$) of atmospheric CO_2 concentration ($[CO_2]$) recorded from Point Barrow (BRW); (b) NDVI and growing season length (GSL). Because decreased $[CO_2]_{min}$ contributes positive effect on enhanced $[CO_2]_{amplitude}$, we show the subtractive $[CO_2]_{min}$ trends in panel (a).

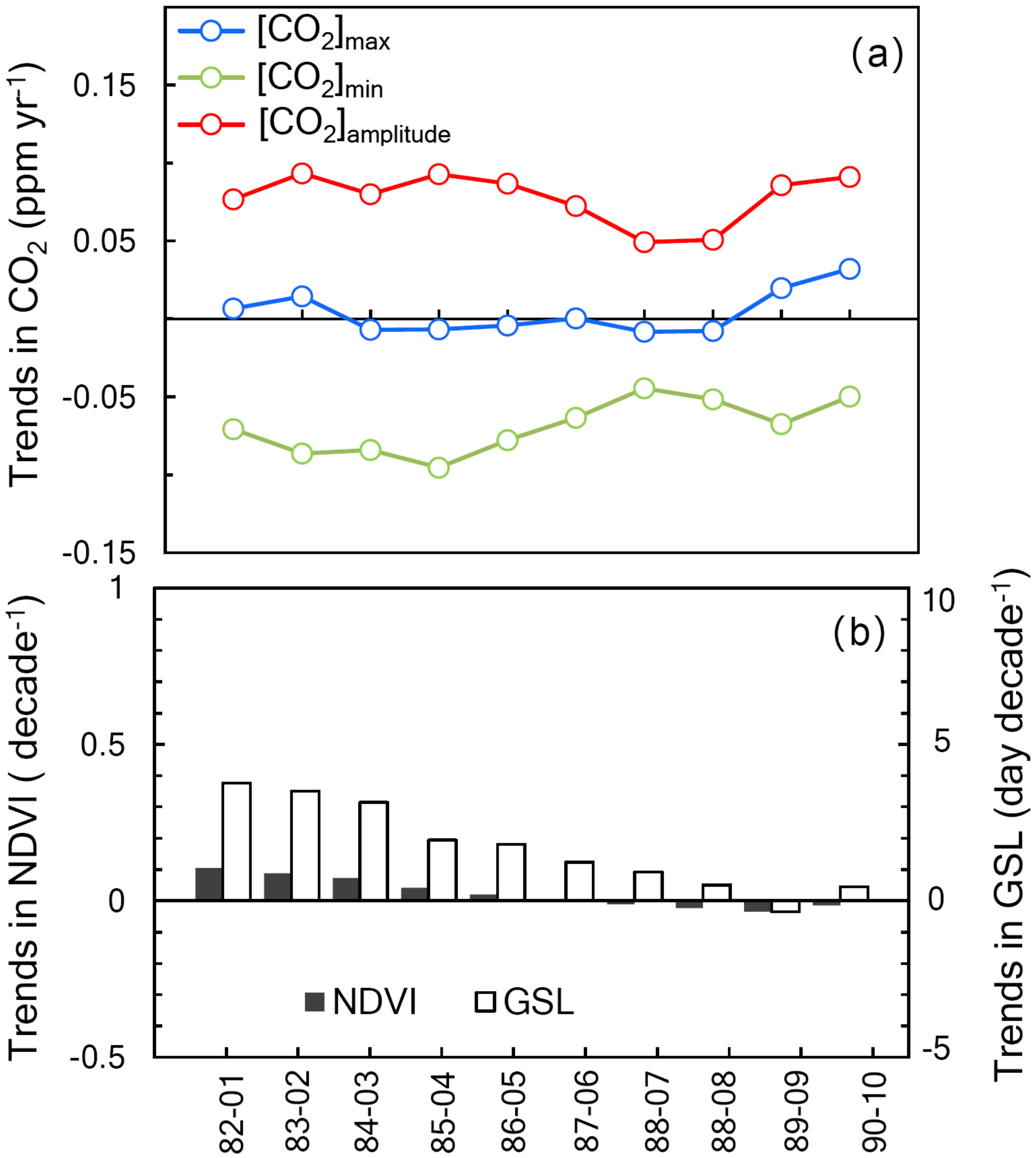

Figure S5. Temporal variation of (a) atmospheric $[CO_2]_{amplitude}$; (b) $[CO_2]_{min}$; (c) $[CO_2]_{max}$ at BRW; (d) NDVI; (e) GPP (MTE); (f) growing season NEE; in northern lands (>50 °N); over 1982-2010. In each panel, the disperse dots showed the anomalies of each metrics, the dashed black line with the grey shade areas indicated the 5-year dynamics (mean ±1 S.D.). The changing trends of each metrics during 1982-2010 and 1993-2007 were estimated by Theil-Sen estimator which were respectively shown by red and blue lines. The NEE data were extracted from the ref (Belshe et al., 2013), which collected observational data on CO_2 flux from 52 studies spanning 32 sites across tundra areas (northern 50 °N) from1982 to 2010.We selected the site-year flux measurements for growing season (Note that the positive values mean CO_2 uptake).

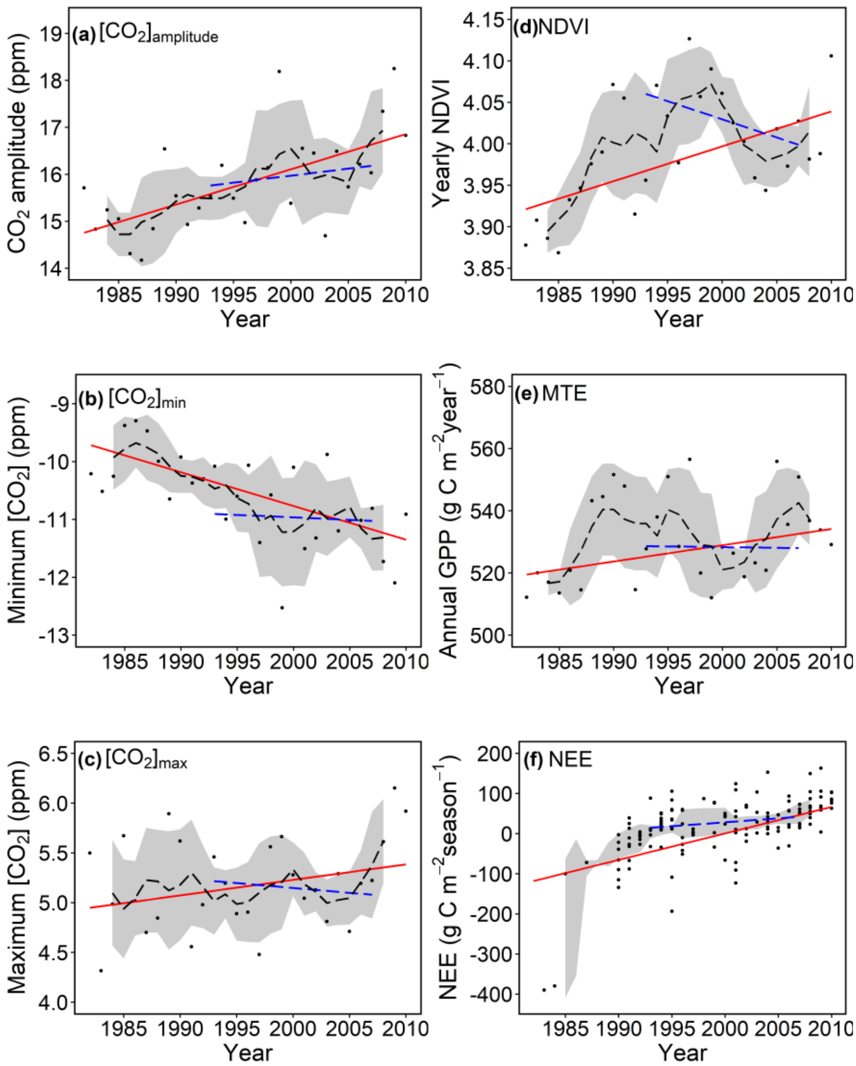

Figure S6. The correlation between NDVI and GSL in temporal and spatial scales. (a), The linear correlation between the average NDVI and GSL anomalies across northern lands (>50 °N), from 1982 to 2010 (R^2 = 0.80, P < 0.001). (b), Spatial distribution of the correlation coefficient (*r*) between NDVI and GSL anomalies over 1982–2010 (if the *P* value for a grid cell was >0.1, we determined that the correlation was insignificant and set its coefficient as zero).

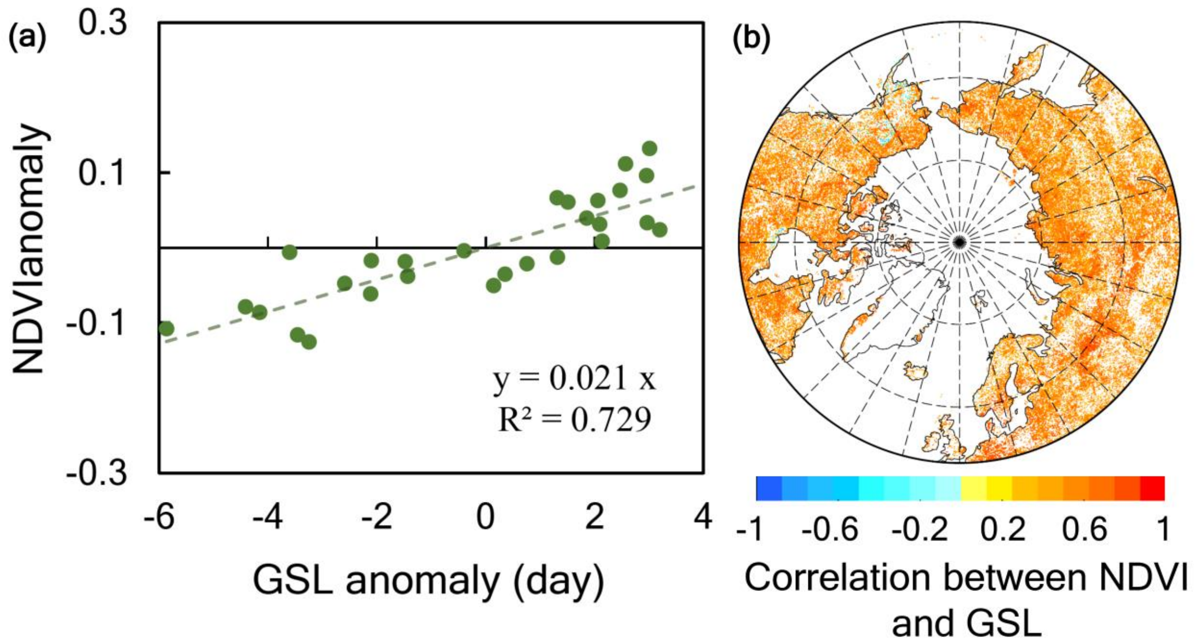

Figure S7. Response of SOS and EOS to seasonal temperature in northern high latitude during 1982-2010. Partial correlation coefficients between (a), SOS and spring temperature (b), EOS and autumn temperature during 1982-2010. Note that the negative partial correlation coefficients in panel (a) represent that warmer spring advances the start of growing season, and the positive coefficients in panel (b) means the delayed end of growing season with warmer autumn.

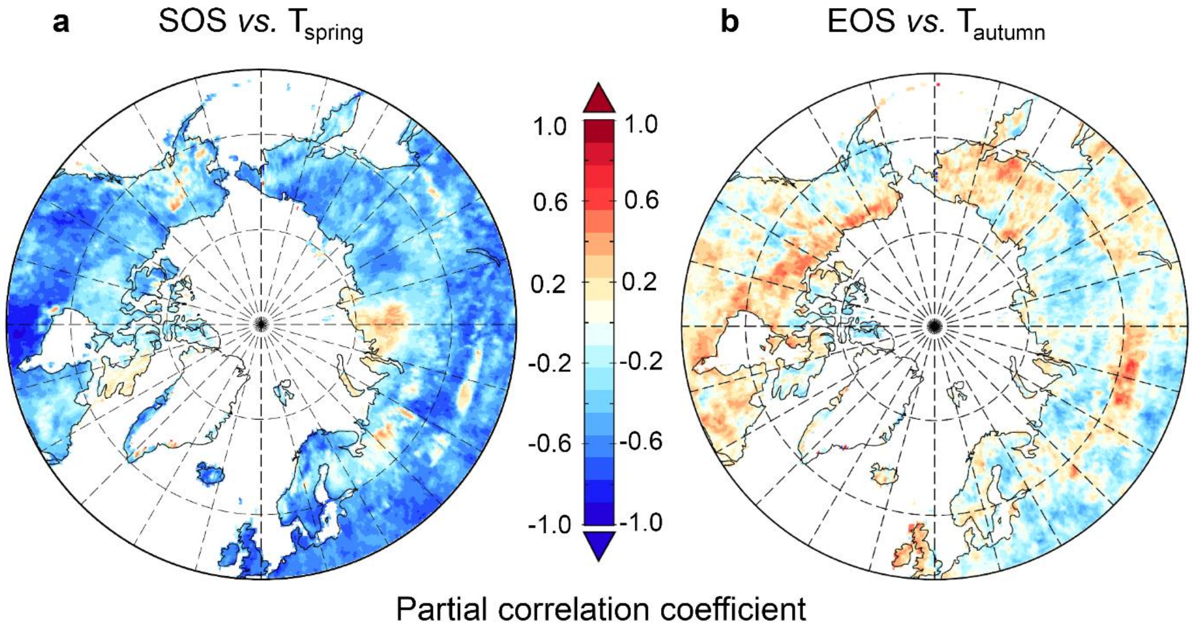

Figure S8. The temporal dynamics of NDVI and phenological metrics in northern high latitudes during 1982-2010. The broken and dashed lines showed the anomalies and 5-year moving means of (a), NDVI and GSL; (b), SOS and EOS. The colors linked *Y*-axis with respective metrics. The 15-year moving trends of each metric were shown in panel (c). Note that the temporal variation and changing rates of NDVI is magnified 10 times to arrive at the same magnitude of GSL, SOS and EOS.

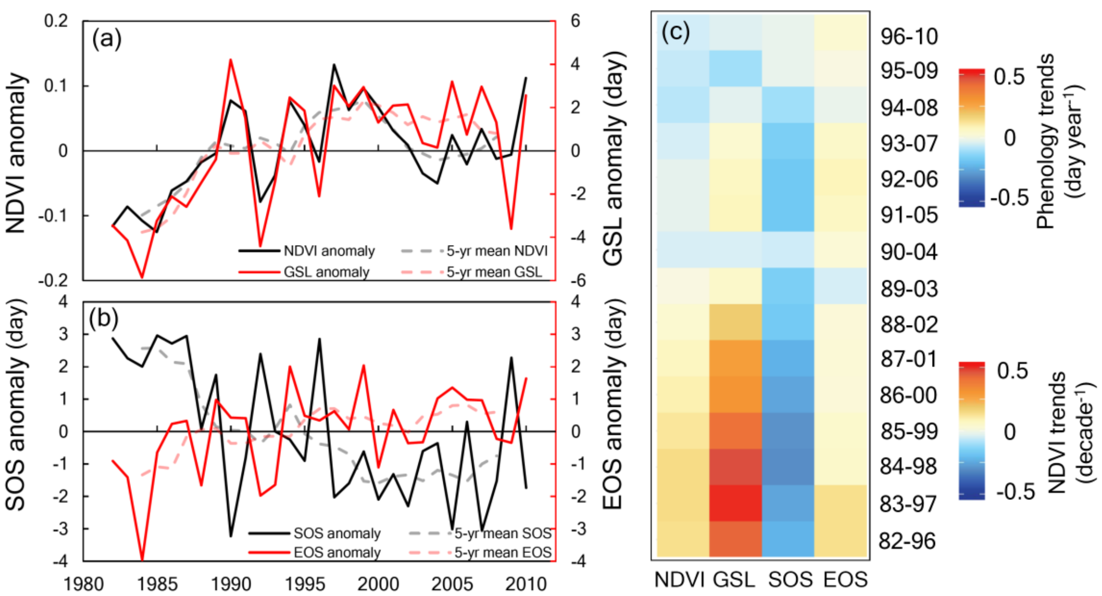

Figure S9. The partial correlation coefficient (partial *r*) of NDVI and model GPP to spring temperature over northern lands (>50 °N) during 1982-2010. The spatial maps of (a) the partial *r* between NDVI and spring temperature; and (b) the partial r between model GPP and spring temperature averaging from the five terrestrial models. The pdfs of partial r between NDVI and spring temperature (green line) and the partial r between model GPP and spring temperature (blue line).

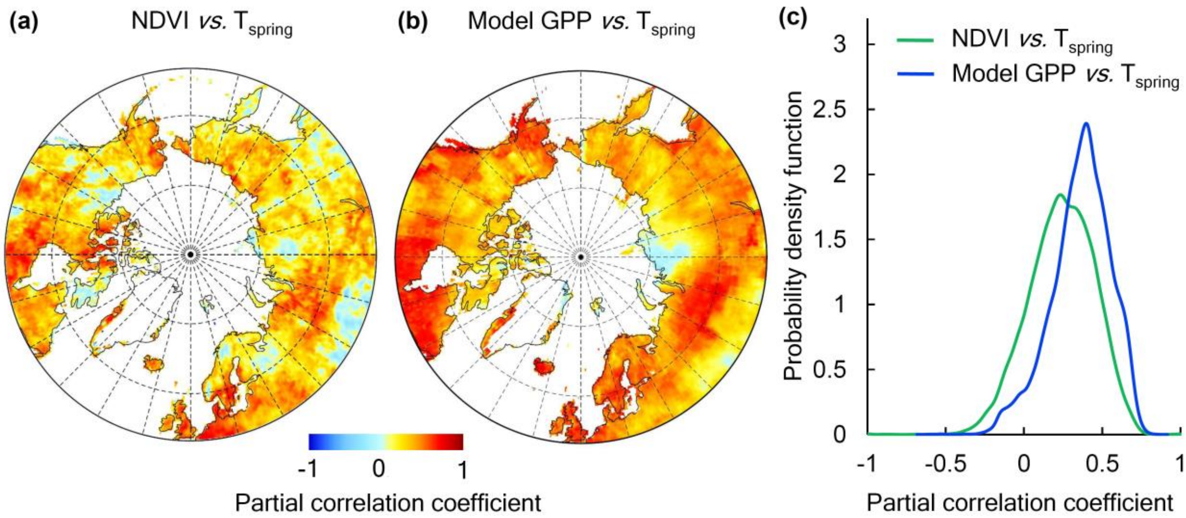

Figure S10. The partial correlation coefficient (partial *r*) of NDVI and model GPP to autumn temperature over northern lands (>50 °N) during 1982-2010. The spatial maps of (a) the partial *r* between NDVI and autumn temperature; and (b) the partial r between model GPP and autumn temperature averaging from the five terrestrial models. The pdfs of partial r between NDVI and autumn temperature (green line) and the partial r between model GPP and autumn temperature (blue line).

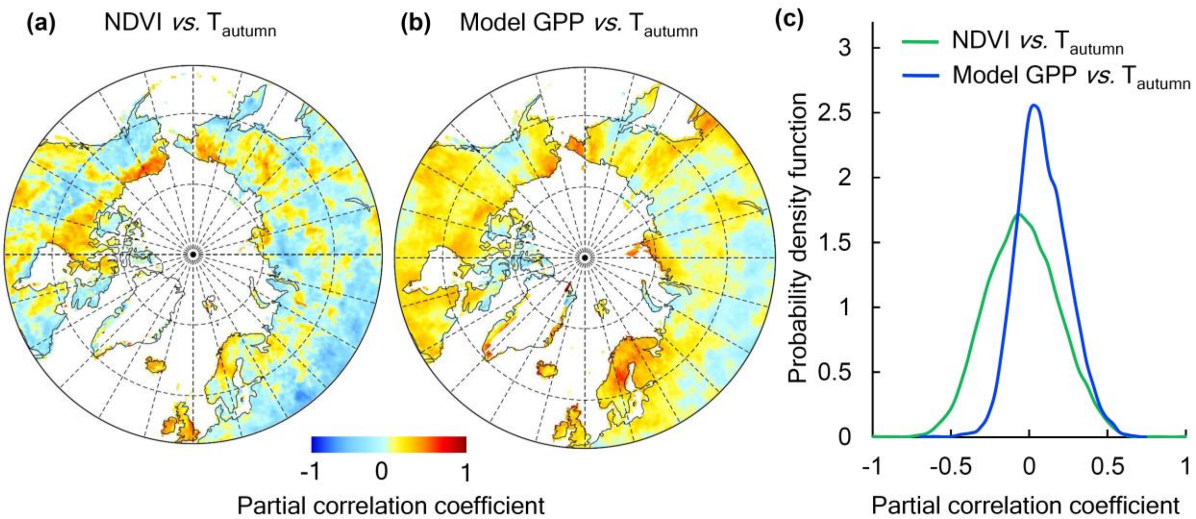

Figure S11. The trends of seasonal respiration over northern lands (>50 °N) during the whole studied periods (1982-2010) and the special periods (1993-2007). FLUXCOM daily respiration was used here to calculate growing-season and non-growing season respiration following the NDVI determined growing-season length (see Text S1). The green bins showed the linear trends of respiration in growing-season and non-growing season over the period of 1982-2010. And the bins with black represented the trends of seasonal respiration during 1996-2010. ***Significant difference at *P* <0.01.

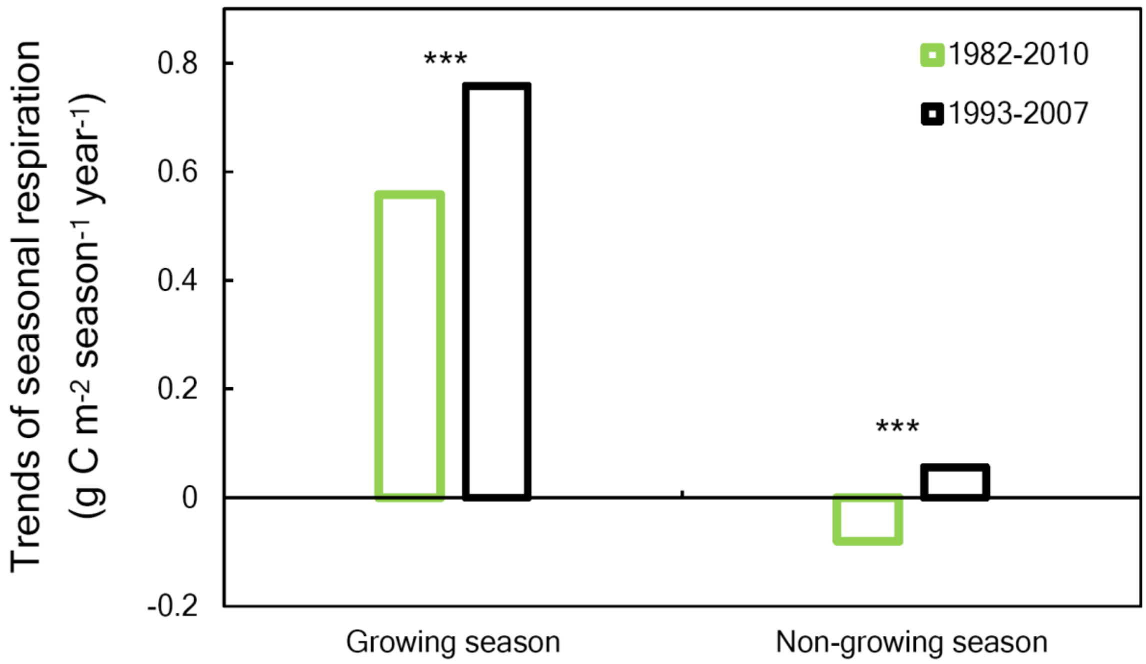

Table S1. Information of the ensemble terrestrial ecosystem models**.**

Model	Reference	Time interval	Phenology module	Phenology determination
ORCHIDEE	Krinner et al., 2005	1982-2009	STOMATE(Ball et al.,1987)	Warmth and/or moisture stress criteria(depend on the PFT)
CLM4.5	Oleson et al., 2013; Koven et al., 2013	1982-2005	GDD (White et al., 1997)	cold and drought stress
CoLM	Dai et al., 2003; Ji et al. 2014	1982-2006	Adapted from Kucharik et al. 2000	Warmth and/or moisture stress criteria (depend on the PFT)
Uvic	H. D. Matthews et al.,2004	1982-2009	Climate coupled TRIFFID [Cox PM (1999)]	Temperature-dependent leaf turnover rate
TEM6	Euckirchen et al.,2006	1982-2009	STM(Zhuang et al.,2001; Goodrich,1976)	The length of the annual non-frozen period

Table S2 The 10-year moving trend of $[CO_2]_{amplitude}$, $[CO_2]_{max}$ and $[CO_2]_{min}$ at BRW over 1982-2010**.**

	$[CO_2]_{amplitude}$ (ppm year^{-1})		$[CO_2]_{max}$ (ppm year^{-1})		$[CO_2]_{min}$ (ppm year^{-1})	
	Coefficient	*P*	Coefficient	*P*	Coefficient	*P*
1982-1991	-0.020	1.000	0.015	1.000	-0.018	0.858
1983-1992	0.050	0.371	0.030	0.858	-0.047	0.592
1984-1993	0.061	0.323	-0.006	0.858	-0.088	0.210
1985-1994	0.163	0.088	-0.011	0.858	-0.166	0.020
1986-1995	0.163	0.088	0.006	1.000	-0.145	0.032
1987-1996	0.089	0.419	0.006	1.000	-0.070	0.283
1988-1997	0.030	0.653	-0.106	0.210	-0.076	0.283
1989-1998	0.008	0.928	-0.106	0.210	-0.053	0.592
1990-1999	0.158	0.088	0.014	0.858	-0.171	0.074
1991-2000	0.140	0.152	0.078	0.283	-0.046	0.592
1992-2001	0.126	0.210	0.014	0.721	-0.100	0.283
1993-2002	0.114	0.283	0.014	1.000	-0.103	0.283
1994-2003	0.032	1.000	-0.008	1.000	0.016	0.858
1995-2004	0.103	0.474	0.028	0.592	0.008	1.000
1996-2005	0.058	0.858	-0.045	0.721	0.027	0.858
1997-2006	-0.020	0.858	-0.048	0.592	0.074	0.283
1998-2007	-0.068	0.474	-0.051	0.210	0.098	0.371
1999-2008	-0.060	0.858	-0.006	1.000	0.089	0.474
2000-2009	0.213	0.210	0.081	0.152	-0.111	0.474
2001-2010	0.150	0.283	0.103	0.020	0.022	0.858

Table S3. The 15-year moving trend of $[CO_2]_{amplitude}$, $[CO_2]_{max}$ and $[CO_2]_{min}$ at BRW over 1982-2010**.**

	$[CO_2]_{amplitude}$ (ppm year^{-1})		**$[CO_2]_{max}$** (ppm year^{-1})		**$[CO_2]_{min}$** (ppm year^{-1})	
	Coefficient	*P*	Coefficient	*P*	Coefficient	*P*
1982-1996	0.033	0.400	-0.006	0.843	-0.031	0.276
1983-1997	0.069	0.067	-0.011	0.692	-0.077	0.075
1984-1998	0.085	0.067	-0.011	0.488	-0.092	0.018
1985-1999	0.140	0.015	-0.007	0.843	-0.141	0.002
1986-2000	0.130	0.033	0.019	0.621	-0.102	0.018
1987-2001	0.126	0.033	0.014	0.621	-0.100	0.023
1988-2002	0.103	0.067	0.005	1.000	-0.086	0.048
1989-2003	0.049	0.656	-0.026	0.373	-0.046	0.488
1990-2004	0.085	0.151	0.003	1.000	-0.066	0.235
1991-2005	0.077	0.166	0.007	0.921	-0.046	0.428
1992-2006	0.052	0.276	-0.013	0.767	-0.041	0.488
1993-2007	0.030	0.553	-0.010	0.767	-0.009	0.767
1994-2008	0.051	0.373	0.019	0.488	-0.020	0.692
1995-2009	0.113	0.092	0.034	0.138	-0.058	0.373
1996-2010	0.103	0.092	0.054	0.092	-0.030	0.692

Table S4. The changing trends of seasonal temperature from 1982 to 2010 across 15-year intervals (the linear regression results in Figure3 c)**.**

	Spring (℃ year^{-1})		**Summer**(℃ year^{-1})		**Autumn**(℃ year^{-1})		**Winter**(℃ year^{-1})	
	Coefficient	P	Coefficient	P	Coefficient	P	Coefficient	P
1982-1996	0.114	0.029	0.032	0.166	0.000	1.000	0.044	0.553
1983-1997	0.114	0.013	0.033	0.166	0.037	0.428	0.069	0.198
1984-1998	0.117	0.013	0.027	0.276	0.011	0.767	0.047	0.428
1985-1999	0.116	0.013	0.049	0.113	0.044	0.488	0.066	0.235
1986-2000	0.087	0.092	0.043	0.166	0.044	0.553	0.067	0.235
1987-2001	0.072	0.138	0.036	0.276	0.043	0.553	0.051	0.428
1988-2002	0.049	0.322	0.031	0.276	0.065	0.322	0.047	0.428
1989-2003	0.012	0.692	0.024	0.322	0.044	0.276	0.044	0.488
1990-2004	0.008	0.767	0.041	0.092	0.098	0.029	0.051	0.166
1991-2005	-0.048	0.553	0.034	0.198	0.101	0.013	0.048	0.322
1992-2006	0.020	0.488	0.049	0.060	0.108	0.010	0.046	0.373
1993-2007	0.009	0.692	0.061	0.023	0.108	0.013	-0.010	0.921
1994-2008	-0.006	0.921	0.038	0.092	0.074	0.138	0.039	0.621
1995-2009	-0.027	0.621	0.020	0.373	0.014	0.843	0.079	0.138
1996-2010	-0.033	0.322	0.018	0.488	0.023	0.553	0.018	0.767

Table S5. The changing trends of GSL, SOS and EOS during 1982-2010 by 15-year intervals (the linear regression results in Figure S7).

	GSL (day year^{-1})		**SOS**(day year^{-1})		**EOS**(day year^{-1})	
	Coefficient	P	Coefficient	P	Coefficient	P
1982-1996	0.441	0.013	-0.228	0.060	0.134	0.060
1983-1997	0.510	0.008	-0.257	0.048	0.134	0.048
1984-1998	0.476	0.010	-0.304	0.023	0.055	0.023
1985-1999	0.403	0.018	-0.293	0.023	0.049	0.023
1986-2000	0.317	0.075	-0.256	0.029	0.020	0.029
1987-2001	0.273	0.113	-0.231	0.048	0.024	0.048
1988-2002	0.180	0.198	-0.170	0.060	0.019	0.060
1989-2003	0.054	0.621	-0.152	0.198	-0.044	0.198
1990-2004	-0.041	0.843	-0.052	0.621	0.026	0.621
1991-2005	0.079	0.276	-0.176	0.060	0.068	0.060
1992-2006	0.069	0.428	-0.176	0.166	0.087	0.166
1993-2007	0.041	0.553	-0.152	0.138	0.057	0.138
1994-2008	-0.029	0.921	-0.102	0.276	-0.021	0.276
1995-2009	-0.100	0.621	-0.023	1.000	-0.003	1.000
1996-2010	-0.034	0.843	-0.023	0.921	0.034	0.921

References

Ball, J. T., Woodrow, I. E. & Berry, J. A. (1987) A model predicting stomatal conductance and its contribution to the control of photosynthesis under different environmental conditions. In Progress in photosynthesis research 221-224.

Cox, P. et al. (1999) The impact of new land surface physics on the GCM simulation of climate and climate sensitivity. Clim Dynam **15**, 183-203.

Dai, Y. et al. (2003) The Common Land Model. B *Am Meteorol Soc* 84, 1013-1023.

Goodrich, L. E. (1976) A numerical model for assessing the influence of snow cover on the ground thermal regime. PhD thesis, McGill University, Montreal. Canada, **410**.

Jung, M., M. Reichstein, H. A. Margolis, et al. (2011) Global patterns of land-atmosphere fluxes of carbon dioxide, latent heat, and sensible heat derived from eddy covariance, satellite, and meteorological observations. *J. Geophys Res* **116**,001566.

Jung, M., M. Reichstein, C. R. Schwalm, et al. (2017) Compensatory water effects link yearly global land CO_2 sink changes to temperature. *Nature* **541**, 516-520.

Koven, C. D., Riley, W. J. & Stern, A. (2013) Analysis of Permafrost Thermal Dynamics and Response to Climate Change in the CMIP5 Earth System Models. *J. Climate* **26**, 1877-1900.

Kucharik, C. J. et al. (2000) Testing the performance of a dynamic global ecosystem model: Water balance, carbon balance, and vegetation structure. *Global Biogeochem. Cy* **14**, 795-825.

Lasslop, G., M. Reichstein, D. Papale, et al. (2010) Separation of net ecosystem exchange into assimilation and respiration using a light response curve approach: critical issues and global evaluation. *Global Change Biol* **16**, 187-208.

Oleson, K. W. et al. (2010) Technical description of version 4.0 of the Community Land Model (CLM). NCAR Tech[R]. Note NCAR/TN-4781STR, **25**.

Papale, D., and R. Valentini. (2003). A new assessment of European forests carbon exchanges by eddy fluxes and artificial neural network spatialization. *Global Change Biol* **9**, 525-535.

Reichstein, M., E. Falge, D. Baldocchi, et al. (2005) On the separation of net ecosystem exchange into assimilation and ecosystem respiration: review and improved algorithm. *Global Change Biol* **11**, 1424-1439.

Taylor, K. E., R. J. Stouffer, and G. A. Meehl. (2012) An Overview of CMIP5 and the Experiment Design. *B Am Meteorol Soc* **93**, 485-498.

Tramontana, G., K. Ichii, G. Camps-Valls, E. Tomelleri, and D. Papale. (2015). Uncertainty analysis of gross primary production upscaling using Random Forests, remote sensing and eddy covariance data. *Remote Sens Environ* **168**, 360-373.

Tramontana, G., M. Jung, C. R. Schwalm, et al. (2016) Predicting carbon dioxide and energy fluxes across global FLUXNET sites with regression algorithms. *Biogeosciences* **13**, 4291-4313.

Van Vuuren, D. P., J. Edmonds, M. Kainuma, et al. (2011) The representative concentration pathways: an overview. *Climatic Change* **109**, 5-31.

Zhuang, Q., Romanovsky, V. E. & McGuire, A. D. (2001) Incorporation of a permafrost model into a large-scale ecosystem model: Evaluation of temporal and spatial scaling issues in simulating soil thermal dynamics. *J. Geophys Res: Atmospheres* **106**, 33649-33670.